ECS Transactions, 45 (24) 89-95 (2013)
10.1149/04524.0089ecst ©The Electrochemical Society

Finite-Element Computer Simulations on Cyclic Voltammograms Measured at Recessed Nanodisk-Array Electrodes

Khanh-Hoa Tran-Ba and Takashi Ito

Department of Chemistry, Kansas State University, Manhattan, Kansas 66506, USA

The characteristics of cyclic voltammograms (CVs) at recessed nanodisk-array electrodes (RNEs) were investigated using finite-element computer simulations. Simulations were performed for RNEs based on planar electrodes coated with electrically-insulating films comprising hexagonally-distributed, vertically-oriented cylindrical nanopores (12 nm in radius, 30 nm deep). CVs and concentration profiles of redox species were simulated by varying electrode spacing (2*s*) and the diffusion coefficient of a redox species within the nanopores (D_{pore}). For nm-scale *s* and large D_{pore}, peak-shaped CVs with currents very similar to those at a film-free electrode were obtained due to the overlapping of diffusion layers extended from multiple electrodes. However, larger *s* and smaller D_{pore} gave smaller peak currents, as the nanoscale electrodes limited the number of redox species to be reacted. Further increase in *s* offered sigmoidal CVs though *s* was small enough for the overlapping of diffusion layers. These trends were consistent with experimental CVs measured at RNEs.

Introduction

A recessed nanodisk-array electrode (RNE) consists of an array of nanoscale disk electrodes formed at the bottom of uniform cylindrical nanopores (**Figure 1a**). RNEs have been fabricated by covering planar electrodes with electrically insulating nanoporous films such as track-etched polymer membranes (TEPM) (1, 2), nanoporous anodic alumina membranes (NAAM) (3-6), and block copolymer-derived films (7-11). In electroanalytical studies, the underlying electrodes can be used as electrochemical detectors. The nanopores define molecular pathways onto the underlying disk electrodes. Thus, their permeability modulated by physical blocking (5, 6), surface charge (2, 8, 9) and swelling of the nanoporous materials (11) can be assessed by measuring the faradic current of redox species dissolved in solution. The uniform size of nanopores in a RNE provides a means for designing electrochemical sensors with selectivity based on the size, charge and chemical properties of molecular analytes. RNEs were also employed to investigate diffusion of redox amphiphiles in bilayer assemblies immobilized on the nanopore surface (12).

The cylindrical shape of RNE nanopores, in addition to the assumption of hexagonal nanopore distribution (**Figure 1a**), offers a simple model geometry that facilitates computer simulations of electrochemical data obtained at these electrodes (13, 14). It is reported that the shapes of cyclic voltammograms (CVs) at RNEs depend on the voltage scan rate (*v*), spacing between adjacent nanopores (electrodes) (2*s*) and pore dimensions (pore length, *L*, and radius, *a*) (1, 4, 14). Observations of peak-shaped and sigmoidal

CVs originate from the involvements of the linear and radial diffusion of redox species toward underlying disk electrodes, respectively (**Figure 1b**). The diffusion modes can be qualitatively assessed by comparing the dimensions of RNEs with the diffusion layer thickness ($L_{diffusion}$) that is determined by v and the diffusion coefficients of the redox species inside and outside the nanopores (D_{pore} and D_{bulk}, respectively). Peak-shaped CVs are observed when only redox species initially present within individual nanopores can react on the electrode ($L_{diffusion} < L$; i)) or when diffusion layers extended from adjacent electrodes overlap ($L_{diffusion} > L$ and $L_{diffusion} > s$; iii)). Sigmoidal CVs are observed when the diffusion layers expanded from nanopores do not overlap ($L < L_{diffusion} < s$; ii)). For the μm-scale counterparts of RNEs, computer simulations based on well-established theoretical models (15) offer consistent results with experimental CVs (16, 17).

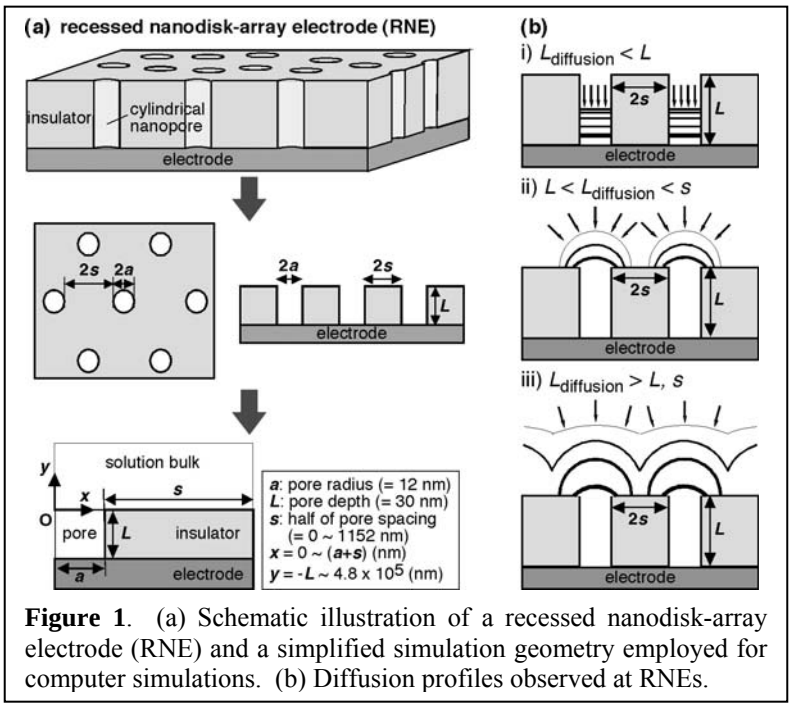

Figure 1. (a) Schematic illustration of a recessed nanodisk-array electrode (RNE) and a simplified simulation geometry employed for computer simulations. (b) Diffusion profiles observed at RNEs.

In contrast, we have found that CVs at RNEs based on polystyrene-poly(methylmethacrylate) diblock copolymer (PS-*b*-PMMA)-derived nanoporous films (11-30 nm in pore diameter, 25-40 nm thick) cannot fully be explained by the theories established for recessed microelectrode arrays (8, 18). These RNEs provided quasi-reversible, peak-shaped CVs, as their nanopore densities were high enough for the overlapping of diffusion layers (*i.e.*, $L_{diffusion} > L$ and $L_{diffusion} > s$). In addition, the difference in redox peak potential (ΔE_p) measured at these electrodes was close to that at a bare gold electrode. However, the peak currents were significantly smaller than those at film-free electrodes with the same geometric area. This marks a sharp contrast to the prediction based on the theoretical models for the recessed microelectrode arrays (15). Based on the comparison of the electrode and pore dimensions in the RNEs and their μm-scale counterparts, it can be hypothesized that the smaller current obtained at the RNEs results from the nanoscale size of the electrodes and/or the molecular permeability of the nanopores reflecting molecule-nanopore interactions.

In this study, finite-element computer simulations with COMSOL Multiphysics® were employed to understand the characteristics of CVs at RNEs, including the observation of peak-shaped CVs with smaller faradic currents. Simulated CVs and the concentration profiles of redox species dissolved in solution were systematically obtained for different s and D_{pore}. The concentration profiles revealed possible mechanisms that led to the smaller peak currents in CVs measured at the RNEs. Furthermore, this study provided insight into conditions required to design chemical sensors based on the physical blocking of RNE nanopores with analytes.

Experimental

COMSOL Multiphysics® ver 4.3 with the CFD Module operated on a Dell Optiplex GX520 (Pentium 4 CPU, 3 GHZ, 4 GB RAM) was employed for the simulations. Details of the simulation procedure, including the equations for Fick's law, electrode reaction kinetics and mass balance equations as well as the mesh of a simulation cell, are described previously (13). The simulation geometry of a RNE (a = 12 nm, L = 30 nm) is shown in **Figure 1a**, which corresponds to a RNE based on a PS-*b*-PMMA-derived nanoporous film that was previously studied by our group (9, 10, 13). The nanopore radius is significantly larger than the sizes of water molecules and ions, making it possible to carry out computer simulations based on continuum theory (19). Simulated CVs were obtained for a reversible, uncharged redox species (at 3 mM), which corresponded to 1,1'-ferrocenedimethanol (D_{bulk} = 6.4 x 10^{-6} cm^2/s (20)). The diffusion coefficients of the species in the oxidized and reduced forms were assumed to be the same. The potential interval for current recording was 2 mV. Computer simulations were carried out (1) for different s (0 ~ 1152 nm), where s = 0 corresponds to a bare electrode (with no nanoporous film) and s = 22 nm was estimated from CVs of the adsorbed cytochrome c (13), and (2) for different D_{pore}. Simulated CVs (at v = 0.05 V/s; $L_{diffusion}$ = 26 μm) show current density defined by the geometric electrode area as a function of overpotential (= $E - E^0$). At the RNEs studied here, the diffusion layer thickness ($L_{diffusion}$) was much larger than the nanopore depth (L = 30 nm). The concentration profiles were shown for redox species in the reduced form, i.e., one that was initially added to the solution.

Results and Discussion

CVs and Concentration Profiles at RNEs with Different *s*

Figure 2a shows simulated CVs at RNEs with different s under the assumption of $D_{pore} = D_{bulk}$ (13). Quasi-reversible ($\Delta E_p \leq 75$ mV), peak-shaped CVs are obtained for the relatively small s ($\leq$ 144 nm) due to the diffusion layer overlapping as expected from $L_{diffusion} > L$ and $L_{diffusion} > s$. At very small s ($\leq$ 72 nm), CVs are almost identical to that at the bare electrode (s = 0 nm), as anticipated from the theory for recessed microelectrode arrays (15, 16). However, a further increase in s leads to a gradual decrease peak current and then to a sigmoidal CV, even though s is much smaller than $L_{diffusion}$. The CV at s = 288 nm is less reversible as shown by the relatively large ΔE_p, (= 97 mV), and that at 1152 nm is almost sigmoidal.

These changes in CV can be understood by comparing the concentration profiles of redox species obtained at the different s (**Figure 2b**). It should be noted that, in these profiles, the scale of the ordinate (0 ~ 480 μm) is much larger than that of the abscissa (nm-scale), and thus the RNE nanopore present at x = 0 ~ 12 nm cannot be seen. At s = 22 nm, redox species near the RNE surface, including the region just above the insulator layer, is completely converted to its oxidized form at E_{high} (i.e., C_{Red} = 0 M and C_{ox} = 3 mM, shown in black in the profiles). The concentration profiles are identical to those obtained at a bare electrode (s = 0 nm), resulting in the observation of the identical CVs (**Figure 2a**). At s = 288 nm, the concentration of the oxidized/reduced forms is independent of x, giving a linear diffusion profile. However, the diffusion layer of the

oxidized species at E_{high} is significantly thinner than that at s = 0 nm, indicating that less redox species can be oxidized at the electrode. The concentration profile explains the observation of the peak-shaped CV with a smaller faradic current: The smaller faradic current is due to the smaller concentration change originating from the limited number of redox species that can be reacted at the nanoscale electrode during the timescale of the CV measurement. At s = 1152 nm, changes in the concentration of the redox species is significantly smaller. Unfortunately, it is unclear whether the diffusion profile is radial in these profiles, but the small concentration change around the nanoscale electrode may lead to sigmoidal CV. This result is consistent with experimental CVs measured at TEPM-based RNEs (1).

These results show that the s-dependence of CVs at RNEs is different from that at their μm-scale counterparts. The nanoscale size of the electrode in a RNE limits the number of redox species to be reacted at the electrode, resulting in observations of peak-shaped CVs with smaller faradic currents as well as sigmoidal CVs even at $L_{diffusion} > s$.

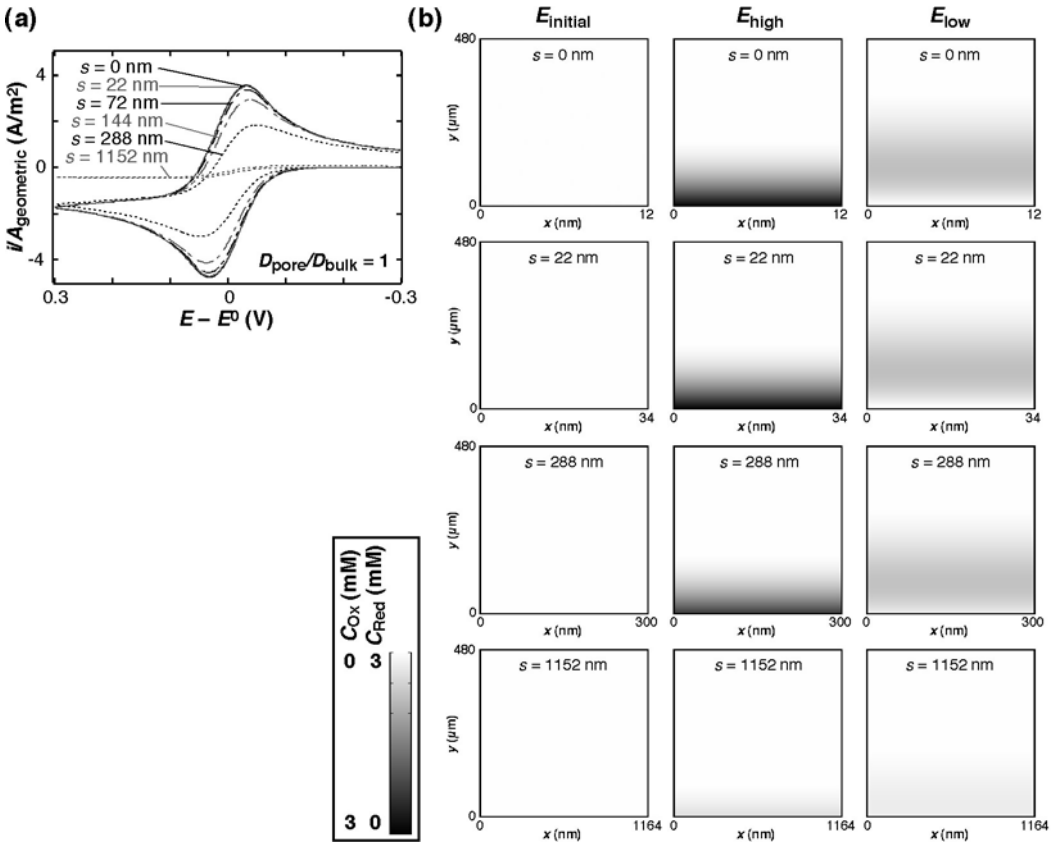

Figure 2. (a) Simulated CVs at RNEs with different s ($D_{pore} = D_{bulk}$). (b) Concentration profiles of the redox species at $E_{initial}$, E_{high} and E_{low} ($E - E^0$ = -0.3, +0.3 and -0.3 V, respectively) for four different s (= 0, 22, 288 and 1152 nm). Note that the electrode is located at $x = 0 \sim 12$ nm.

CVs and Concentration Profiles at RNEs for Different D_{pore}

Figure 3a shows simulated CVs for different D_{pore} at fixed s (= 22 nm). Peak-shaped CVs with similar ΔE_p (< 70 mV) are obtained at $D_{pore} \geq 0.1\ D_{bulk}$, whereas the peak current is smaller at $D_{pore} < 0.1\ D_{bulk}$. The concentration profiles at E_{high} (**Figure 3b**) show that less redox species are reacted at the electrode with decreasing D_{pore}, which explains the smaller faradic current. The smaller concentration change originates from

the smaller flux of the redox species through the nanopore due to the smaller D_{pore}. The *x*-independent diffusion profile originating from the overlapped diffusion layers leads to the observation of a peak-shaped CV. On the other hand, sigmoidal CVs are obtained at D_{pore} = 0.001 D_{bulk}, although peak-shaped CVs should be obtained regardless of D_{pore} according to the model shown in **Figure 1b**. The results at the very small D_{pore} may be due to the limited mesh sizes employed for the simulations, as the small D_{pore} results in slower molecular diffusion that requires finer meshes for accurate simulations.

These results show that the peak-shaped CVs with smaller faradic currents could be observed for smaller D_{pore}. The smaller flux through the nanopores limits the number of redox species to be reacted at the bottom electrode.

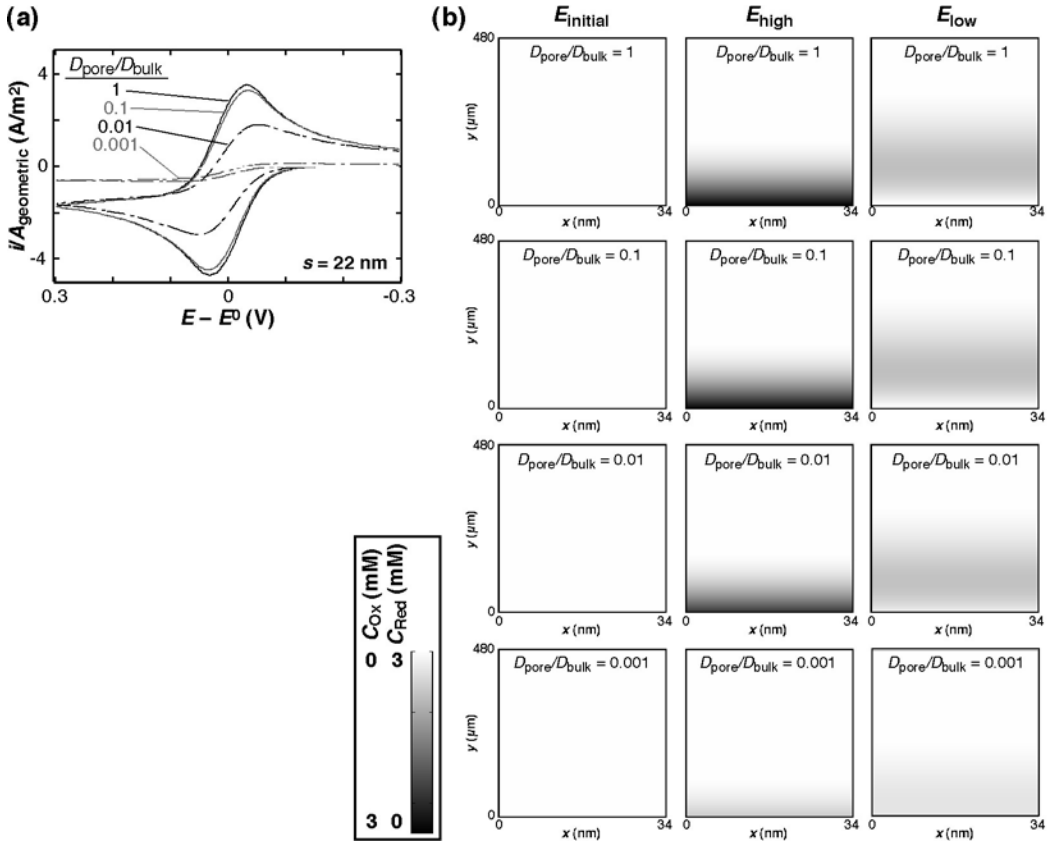

Figure 3. (a) Simulated CVs at RNEs with different D_{pore}/D_{bulk} (*s* = 22 nm). (b) Concentration profiles of the redox species at $E_{initial}$, E_{high} and E_{low} (E - E^0 = -0.3, +0.3 and -0.3 V, respectively) for four different D_{pore}/D_{bulk} (= 1, 0.1, 0.01 and 0.001).

Design of RNE-Based Chemical Sensors

The above results provide insight into the performances of RNE-based electrochemical sensors. Previously, RNEs were applied for electrochemical detections based on changes in nanopore permeability by the following analyte-induced phenomena: (1) physical blocking of RNE nanopores (5, 6), which leads to a decrease in pore density and partial pore radius; (2) swelling of nanoporous films (11), which leads to a decrease in pore radius; and (3) nanopore surface charge changes (2, 8, 9), which leads to changes in effective pore radius due to electrostatic interactions.

The *s*-dependence (**Figure 2a**) clearly shows the presence of an optimum *s* for detection of physical blocking of the RNE nanopores. A decrease in faradic current

induced by physical blocking can be measured for RNEs with relatively large *s*, *i.e*., relatively low pore density. For example, NAAM-based RNEs may show a decrease in faradic current only after many nanopores have been blocked by analytes. These RNEs will not be suitable for trace analysis because many analytes are necessary to reach the optimum pore density, though the sensitivity of the sensors will be primarily determined by the binding strength of surface-immobilized receptors such as antibodies. The relatively low pore density may also be required for detecting permeability changes induced by a decrease in effective nanopore radius. In addition, the D_{pore}-dependence (**Figure 3a**) shows the possibility to develop RNE-based chemical sensors based on changes in chemical environment within the nanopores. For example, D_{pore} depends on solution viscosity in nanopores (21). Thus, RNEs may be applicable for electrochemical detection of analytes that can changes solution viscosity upon their binding to the nanopore surface (*i.e*., binding of polymeric analytes to nanopores coated with polymer brushes).

Conclusion

In this study, finite-element computer simulations are employed to reveal the characteristics of CVs at RNEs. Due to the nanoscale electrode/pore size that limits the number of redox species to be reacted, CVs at RNEs are different from those predicted from the theory established for recessed microelectrode arrays. Peak-shaped CVs with small faradic currents are obtained at RNEs with relatively large *s* (relatively low pore density) and/or with lower D_{pore}. These simulation results make it possible to optimize the properties of RNEs for developing permeability-based electrochemical sensors.

Acknowledgments

This work was funded by the Division of Chemical Sciences, Geosciences, and Biosciences, Office of Basic Energy Sciences of the U.S. Department of Energy (DE-SC0002362). The authors also acknowledge ACS Petroleum Research Funds (ACS PRF# 46192-G5), Terry C. Johnson Center for Basic Cancer Research and Targeted Excellence Funds of Kansas State University for partial financial support of this work.

References

1. T. Ito, A. A. Audi and G. P. Dible, *Anal. Chem.*, **78**, 7048 (2006).
2. D. M. N. T. Perera and T. Ito, *Analyst*, **135**, 172 (2010).
3. C. J. Miller and M. Majda, *J. Am. Chem. Soc.*, **107**, 1419 (1985).
4. C. J. Brumlik, C. R. Martin and K. Tokuda, *Anal. Chem.*, **64**, 1201 (1992).
5. A. de la Escosura-Muniz and A. Merkoci, *Electrochem. Commun.*, **12**, 859 (2010).
6. A. de la Escosura-Muniz and A. Merkoci, *Chem. Commun.*, **46**, 9007 (2010).
7. E. Jeoung, T. H. Galow, J. Schotter, M. Bal, A. Ursache, M. T. Tuominen, C. M. Stafford, T. P. Russell and V. M. Rotello, *Langmuir*, **17**, 6396 (2001).
8. Y. Li, H. C. Maire and T. Ito, *Langmuir*, **23**, 12771 (2007).
9. Y. Li and T. Ito, *Langmuir*, **24**, 8959 (2008).

10. Y. Li and T. Ito, *Anal. Chem.*, **81**, 851 (2009).
11. D. M. N. T. Perera, B. Pandey and T. Ito, *Langmuir*, **27**, 11111 (2011).
12. C. J. Miller, C. A. Widrig, D. H. Charych and M. Majda, *J. Phys. Chem.*, **92**, 1928 (1988).
13. B. Pandey, K. H. Tran Ba, Y. Li, R. Diaz and T. Ito, *Electrochim. Acta*, **56**, 10185 (2011).
14. C. G. Zoski and M. Wijesinghe, *Isr. J. Chem.*, **50**, 347 (2010).
15. C. Amatore, J.-M. Saveant and D. Tessier, *J. Electroanal. Chem.*, **147**, 39 (1983).
16. A. Lavacchi, U. Bardi, C. Borri, S. Caporali, A. Fossati and I. Perissi, *J. Appl. Electrochem.*, **39**, 2159 (2009).
17. T. J. Davies and R. G. Compton, *J. Electroanal. Chem.*, **585**, 63 (2005).
18. H. C. Maire, S. Ibrahim, Y. Li and T. Ito, *Polymer*, **50**, 2273 (2009).
19. H. S. White and A. Bund, *Langmuir*, **24**, 12062 (2008).
20. F.-R. F. Fan, *J. Phys. Chem. B*, **102**, 9777 (1998).
21. R. J. Hunter, *Foundations of Colloid Science*, Oxford University Press, New York (2001).